Structural and functional analyses of the archaeal tRNA m^{2}G/m$^2_2$G10 methyltransferase aTrm11 provide mechanistic insights into site specificity of a tRNA methyltransferase that contains common RNA-binding modules

Akira Hirata[*], Seiji Nishiyama, Toshihiro Tamura, Ayano Yamauchi and Hiroyuki Hori

Department of Materials Science and Biotechnology, Graduate School of Science and Engineering, Ehime University, 3 Bunkyo-cho, Matsuyama, Ehime 790-8577, Japan

ABSTRACT

N^2-methylguanosine is one of the most universal modified nucleosides required for proper function in transfer RNA (tRNA) molecules. In archaeal tRNA species, a specific *S*-adenosyl-L-methionine (SAM)-dependent tRNA methyltransferase (MTase), aTrm11, catalyzes formation of *N^2*-methylguanosine and *N^2,N^2*-dimethylguanosine at position 10. Here, we report the first X-ray crystal structures of aTrm11 from *Thermococcus kodakarensis* (*Tko*), of the apo-form, and of its complex with SAM. The structures show that $_{Tko}$Trm11 consists of three domains: an N-terminal ferredoxinlike domain (NFLD), THUMP domain and Rossmann-fold MTase (RFM) domain. A linker region connects the THUMP-NFLD and RFM domains. One SAM molecule is bound in the pocket of the RFM domain, suggesting that $_{Tko}$Trm11 uses a catalytic mechanism similar to that of other tRNA MTases containing an RFM domain. Furthermore, the conformation of NFLD and THUMP domains in $_{Tko}$Trm11 resembles that of other tRNA-modifying enzymes specifically recognizing the tRNA acceptor stem. Our docking model of $_{Tko}$Trm11-SAM in complex with tRNA, combined with biochemical analyses and pre-existing evidence, provides insights into the substrate tRNA recognition mechanism: The THUMP domain recognizes a 3′-ACCA end, and the linker region and RFM domain recognize the T-stem, acceptor stem and V-loop of tRNA, thereby causing $_{Tko}$Trm11 to specifically identify its methylation site.

INTRODUCTION

Transfer RNA (tRNA) plays a crucial role as the adapter molecule that translates genetic information from messenger RNA (mRNA) to protein. Nascent precursor (pre)-tRNAs must be processed for the maturation of tRNAs. The maturated tRNAs are required for protein synthesis on ribosomes. In the maturation process of archaeal/eukaryotic pre-tRNA molecules, many tRNA maturation factors, which include enzymes and RNA–protein complexes, are responsible for tRNA splicing, processing and modifications.

An enormous number and variety of tRNA modification enzymes have been identified and characterized, and numerous modified nucleosides are more often found in tRNA molecules than in other RNA species (mRNA, ribosomal RNA (rRNA) and small RNA) (1,2). These modified nucleosides are mostly responsible for the stabilization of L-shaped tRNA structure, as well as the fine-tuning of the decoding of mRNAs during translation, and of numerous interactions between RNA and RNA-binding protein partners (3). On the other hand, several modifications are involved in genetic diseases. Deficiencies of tRNA modifications are linked to human genetic diseases, e.g. intellectual disability, Type II diabetes, mitochondrial myopathy and sideroblastic anemia, etc (4,5). Extensive studies of tRNA modification machineries at a molecular level are needed to better understand related human pathologies and provide clues for the design of therapies to treat human genetic diseases.

Methylation is one of the most ubiquitous and abundant kinds of nucleoside modifications and is part of the biosynthetic pathways of the majority of tRNA hypomodifications (1,2,6). In archaea and eukaryotes, small nucleolar (sno) RNAPs in complex with guide sno RNAs produce not only methylation of the 2′-*O* ribose position but also the

[*]To whom correspondence should be addressed. Tel: +81 89 927 9919; Fax: +81 89 927 9919; Email: ahirata@ehime-u.ac.jp

psudouridylation of uridine in tRNA/rRNAs [7]. In most cases, however, specific RNA methyltransferases (MTases) strictly methylate bases and 2′-*O* ribose sugars at precise positions in various RNA species [8]. The RNA MTases are classified into four superfamilies: Rossmann-fold MTase (RFM), SPOUT (SpoU and TrmD), radical-*S*-adenosyl-L-methinonine (SAM) and FAD/NAD(p)-dependent MTase [9]. For tRNA MTases, there are two types designated according to the distinct consumption of the methyl group donor: (i) One is the SAM-dependent tRNA MTases, which are further classified by their catalytic domain [10]; the class I type includes RFM as the catalytic domain, while the class IV type contains the topological-knot structure, which is universally conserved in a member of the SPOUT superfamily [11]. (ii) Second is the folate/FAD/NAD(p)-dependent tRNA MTases, in which TrmFO catalyzes the formation of m^5U54 in tRNA using the 5, 10 methylenetetrahydrofolate as a methyl donor in Gram-positive and some Gram-negative eubacteria [12–14]. Recent studies have elucidated the mechanisms underlying substrate specificity and catalysis of TrmFO [15–19].

The N^2-methylguanosine (m^2G) and N^2, N^2-dimethylguanosine (m^2_2G) are major types of methylated nucleosides. To date, their modifications have been identified at positions 6, 7, 9, 10, 18, 26 and 27 of various tRNAs present in the three domains of life [1,2]. Specific SAM-dependent tRNA MTases have been biochemically and structurally characterized for their methylation at the positions 6, 10, 26 and 27 [20–27]. Bacterial TrmN and archaeal Trm14 play a catalytic role in the formation of m^2G6 nucleoside [20,21]; structural information is available for both, and a mechanism for their site specificity has been proposed based on structure-guided mutagenesis studies [27]. Archaeal Trm-G10 was first identified in *Pyrococcus* species (*Pyrococcus abyssi* (*Pab*) and *Pyrococcus furiosus* (*Pfu*)) and catalyzes the production of m^2G10 or m^2_2G10 nucleosides [28]. Its eukaryotic homolog Trm11 has been shown to catalyze the formation of m^2G10 in tRNA^{Phe} from *Saccharomyces cerevisiae* [29]. Only Trm11, however, is functional when it dimerizes with the 'hub' protein Trm112, which can interact and activate not only Trm11 but also the catalytic subunits of other RNA MTases and translational factor [30,31]. The X-ray crystal structure determination of Trm-G10 or the Trm11-Trm112 complex has not been achieved yet and therefore the structural mechanisms for their site specificity and catalysis remain elusive.

The genes coding for Trm-G10 and Trm11 belong to the cluster of orthologous group COG1041, exclusively and ubiquitously found in archaea and eukaryotes, and the two proteins share ∼30% sequence similarity [28]. Previous reports suggest that Trm-G10 and Trm11 are composed of three domains: an N-terminal ferredoxin like domain (NFLD); a THioUridine synthase, MTase and Pseudouridine synthase domain (THUMP); and a Rossmann-fold MTase catalytic domain (RFM) [28,32–34]. Given the structural and functional similarities of archaeal Trm-G10 and eukaryotic Trm11, we have renamed archaeal Trm-G10 to 'aTrm11' in this study. The naming of aTrm11 is followed by a standard nomenclature for the tRNA MTases, for example, aTrm56 that catalyzes the formation of Cm56

at position 56 of archaeal tRNA [35]. The RFM domain of both Trm11 enzymes is likely to be fused to a THUMP domain that also includes an NFLD responsible for the RNA-binding [28,34,36], and the NFLD is a minimum unit of THUMP domain. Structural studies have revealed that TrmN/Trm14 employ the RFM domain as the catalytic unit, and that one SAM molecule is bound to a pocket of the RFM domain, which is fused to the THUMP domain through a single linker [27]. Similar architectures have been found in other tRNA-modifying enzymes consisting of three domains, i.e. where the NFLD and THUMP domain are fused to one catalytic domain. For examples, CDAT8 is a cytidine deaminase responsible for the deamination of U8 in archaeal tRNA species and composed of the NFLD and THUMP domain fused to one deaminase domain [37]. The biosynthesis of s^4U8 is catalyzed by a 4-thiouridine synthase (ThiI) [32]. ThiI constitutes an NFLD and THUMP domain fused to the pyrophoshatase (PPase) domain through single linker [38,39], although ThiI orthologs from γ-proteobacteria and archaeon *Thermoplasma* species contains a fourth, C-terminal rhodanese-like domain in addition to the three domains [40]. It seems that the two common domains, NFLD and THUMP, confer site specificity to tRNA-modifying enzymes. In fact, TrmN/Trm14, CDAT8, ThiI and aTrm11 were shown to recognize the tRNA acceptor stem required for catalysis [27,34,36,37,41]. Furthermore, it has been shown that a shortened or blunt tRNA ACCA end is deleterious to the activity of ThiI [42] and that the THUMP domain recognizes the 3′-ACCA end of tRNA [43], suggesting that the combination of NFLD and THUMP domains is a key structural module to specify the modification site around the tRNA acceptor stem.

In order to understand the molecular mechanism underlying site specificity of aTrm11, the structural information of aTrm11 should be available. Here, we present the first X-ray crystal structures of aTrm11 from *Thermococcous kodakarensis* (*Tko*), as well as its SAM complex. The $_{Tko}$Trm11 is composed of NFLD and THUMP domains fused to an RFM domain, which is bound to a SAM molecule in its pocket. Our structure-guided mutagenesis identified the SAM binding mode and the putative residues responsible for tRNA-binding. Structural comparison shows that there is a striking similarity between the three domains (NFLD, THUMP and RFM) of $_{Tko}$Trm11 and Trm14 with exception to the conformational location of the RFM domain. Our docking model of a $_{Tko}$Trm11–tRNA complex, combined with biochemical analyses supports previous evidence that the THUMP domain recognizes the 3′-ACCA end that serves as a reference point to measure the distance to the modification site. These findings expand our understanding of the molecular ruler mechanism for site specificity of archaeal Trm11 and Trm14.

MATERIALS AND METHODS

Materials

[Methyl-^{14}C]-SAM (1.95 GBq/mmol) and [methyl-^{3}H]-SAM (2.47 TBq/mmol) were purchased from PerkinElmer. Non-radioisotope-labeled SAM was obtained from Sigma.

DNA oligomers and 2′-*O* methylated primers were obtained from Invitrogen and Hokkaido System Science, respectively. T7 RNA polymerase was purchased from Toyobo. All other chemical reagents were of analytical grade.

Protein preparation and crystallization

Tko cells were prepared following a previously described standard culture protocol (44). The *Tko* genomic DNA was extracted from the cells with a phenol-chloroform mixture. $_{Tko}$Trm11 was assigned as TK0981, N^2, N^2-dimethylguanosine tRNA methyltransferase, in the *Tko* genome project (45). The TK0981 gene was subcloned into a pMD20-T vector using the Mighty TA cloning kit (Takara) and then sequenced. The resulting vector was used as a template to amplify regions of the TK0981 gene by PCR, using the primers listed in Supplementary Table S1. Following NcoI and BamHI digestion, the polymerase chain reaction (PCR) product was ligated into a pET-30a vector (Novagen), which contains the coding sequence for a human rhinovirus 3C (HRV-3C)-cleavable C-terminal His6 tag. The expression vector was used to overexpress the recombinant $_{Tko}$Trm11 in *Escherichia coli* Rosetta 2(DE3) strain (Novagen) cells. *E. coli* cells harboring the vector were grown at 37°C in LB medium supplemented with 50 μg/ml of kanamycin. When the cell density reached OD600 = ∼0.8, isopropylthio-β-galactoside (IPTG) was added to a final concentration of 0.5 mM and cells were grown for an additional 48 h at 20°C. Cells were then harvested by centrifugation at 4320 *xg* at 20°C for 20 min. A total of 7 g of the cells were suspended in 35 ml of buffer A (50 mM Tris-HCl [pH 8.0], 200 mM NaCl and 20 mM imidazole) supplemented with Halt protease inhibitor single-use cocktail (Thermo Scientific) and then disrupted with an ultrasonic disruptor (model VCX-500, Sonics & Materials. Inc, USA). To remove a fraction of *E. coli* proteins by heat denaturation, lysed cells were incubated at 70°C for 45 min and pelleted by centrifugation at 38 900 *xg* at 4°C for 20 min. The supernatant was loaded onto a Ni-NTA Superflow column (Qiagen) equilibrated with buffer A and the enzyme was eluted using buffer A containing 500 mM imidazole. The eluted fractions were collected and loaded onto a HiTrap Heparin-Sepharose column (GE Healthcare) pre-equilibrated with buffer B (50 mM Tris-HCl [pH 8.5], 50 mM KCl and 5 mM 2-mercaptoethanol). The bound protein was eluted with a linear gradient of buffer B containing 50 mM–1 M KCl. The eluted fractions were collected and concentrated to ∼3 ml volume using Vivaspin 15R centrifugal filter units (Sartorius Stedim Biotech). The concentrated protein was applied to a HiLoad 16/60 Superdex 75 pg column (GE Healthcare) equilibrated with buffer C (50 mM Tris-HCl [pH 8.0], 200 mM KCl and 6 mM 2-mercaptoethanol). The fractions corresponding to the single peak eluting between 45–58 ml were collected (Supplementary Figure S1A). For X-ray crystal structure phasing of a selenomethionine substituted (SeMet) crystal of $_{Tko}$Trm11 using the single-wavelength anomalous dispersion (SAD) technique, we found that an additional SeMet was required (data not shown). Therefore, Ile291 was replaced with methionine using the QuickChange site-directed mutagenesis

kit (Stratagene). The mutation was verified by DNA sequencing. The SeMet I291M mutant was expressed by suppression of the biosynthesis pathway for methionine (46) and purified in the same manner as the wild-type (WT) protein. Likewise, we prepared alanine-substituted mutants (I163A, D185A, F187A, D208A, I209A, R210A, D235A and D254A) for the mutagenesis experiment on the SAM-binding site, alanine-substituted mutants (R105A, K106A, R105A/K106A, K122A, R128A, R140A, K122A/R140A, K122A/R128A/R140A, K151A, R152A, K151A/R152A, R266A, K267A, R268A, R266A/K267A/R268A, R317A, K320A and R317A/K320A) for the mutagenesis experiment on the tRNA recognition site, and alanine-substituted mutants (F86A, K87A, V88A, F86A/K87A/V88A, V118A, L120A and V118A/L120A) for the mutagenesis study on the 3′-ACCA end of the tRNA recognition site. Respective protein purities were confirmed by SDS-PAGE with Coomassie staining (Supplementary Figures S1B, S6A, S6C, S6D and S6E).

Respective gel filtration fractions corresponding to the single peak were pooled and concentrated to ∼3 mg/ml using Vivaspin 15R centrifugal filter units. During the concentration of $_{Tko}$Trm11, buffer C was substituted with the crystallization buffer (20 mM Tris-HCl [pH 8.0] and 100 mM NaCl). Initial crystallization trials were set up in VDX48 plates with sealant (Hampton Research) using the hanging-drop vapor diffusion method and commercial crystallization screens from Hampton Research (Index, Salt RX and Crystal screen). The drop solution was equilibrated against 200 μl of reservoir solution at 20°C. A few single crystals of $_{Tko}$Trm11 appeared after ∼6 months with Index screen reagent #12 (i.e. 0.1 M Tris-HCl [pH 8.5] and 3.0 M NaCl). To decrease the growth time of the crystals, we optimized the initial crystallization condition and the concentration of $_{Tko}$Trm11. Full-sized rectangular-shaped (300 × 200 × 200 μm) crystals grew within 2 days when we mixed 2μl of $_{Tko}$Trm11 at 10 mg/ml with an equal volume of crystallization solution composed of 0.1 M Tris-HCl (pH 8.5) and 4.5 M NaCl, and grew crystals at 20°C. SeMet crystals grew under the same conditions. Crystals of $_{Tko}$Trm11 in complex with SAM were obtained by soaking the crystal of $_{Tko}$Trm11 in crystallization mother liquor supplemented with 1 mM SAM at 20°C for 3 h. Cryoprotection was achieved by stepwise transfer to the respective artificial mother liquor containing 15% glycerol. The crystals were then flash-frozen in liquid nitrogen.

Structure determination

X-ray diffraction data sets from apo-$_{Tko}$Trm11 (λ = 1.0000) and $_{Tko}$Trm11-SAM (λ = 1.0000) were recorded at the BL38B1 beamline at SPring-8 (Hyogo, Japan). The SAD data set from SeMet-I291M (λ = 0.9791) was also collected at the same beamline at SPring-8. Data collection statistics are in Table 1. All data sets were processed, merged and scaled using the HKL2000 program (47). Using the deduced Se-SAD data set, all 6 Se positions were identified and refined in the orthorhombic space group $P2_12_12_1$, and the initial phase was calculated using AutoSol in PHENIX (48), and followed by automated model building using RE-SOLVE (49). The resulting map and partial model were

used for manually building the model using COOT (50). The model was further refined using PHENIX (48). Using the refined coordinates of SeMet-I291M as a search model, molecular replacement phasing of the apo-$_{Tko}$Trm11 and $_{Tko}$Trm11-SAM crystal structure was achieved using the Phaser program (51). The model was further built manually with COOT (50) and refined with PHENIX (48). The structures of apo-$_{Tko}$Trm11 and $_{Tko}$Trm11-SAM were refined to R_{work}/R_{free} of 20.5%/24.0% at 1.70 Å resolution and 18.7%/22.3% at 1.74 Å resolution, respectively (Table 1). The crystals belonged to space group $P2_12_12_1$, where one apo-$_{Tko}$Trm11 molecule is present per asymmetric unit. The final model of apo-$_{Tko}$Trm11 contained 323 residues (1–257 and 266–331) and 179 water molecules, and the $_{Tko}$Trm11-SAM contained 323 residues (1–257 and 266–331) and 282 water molecules and one SAM molecule. Both final models were further checked using PROCHECK (52), showing the quality of the refined model. Ramachandran plots (%) of the two structures are tabulated in Table 1. The structure factors and coordinates of apo-$_{Tko}$Trm11 and $_{Tko}$Trm11-SAM have been deposited in the Protein Data Bank (PDB code 5E71 and 5E72).

Preparation of *Tko* tRNA^{Trp} transcript and its mutants (G10A, ΔA, ΔCA, ΔCCA and ΔACCA)

Tko tRNA^{Trp} transcript (Supplementary Figure S2A) was prepared by T7 RNA polymerase *in vitro* transcription using our previously reported method (53) from a DNA template produced from PCR amplification using our designed two primers (F and R denote the upstream and the downstream primers, respectively, and DNA sequences in bold show a promoter that is recognized by T7 RNA polymerase): Tk-TrpF, 5′-**GGGTAATACGACTCACTATA**GGGGGCGTGGTGTAGCCTGGTCCATCATCGCGCGGGCTCCAGACCCGCGG-3′; Tk-TrpR, 5′-TGGTGGGGGCGCGGGGATTTGAACCCCGGTCCGCGGGTCTGGAGCCCG-3′.

The G10A mutant, which replaces guanine at 10 position of *Tko* tRNA^{Trp} transcript with adenine, was prepared as described above by using the following two primers (A10 is underlined): Tk-TrpF, 5′-**GGGTAATACGACTCACTATA**GGGGGCGTGA̲TGTAGCCTGGTCCATCATCGCGCGGGCTCCAḠACCCGCGG-3′; G10A-R, 5′-TGGTGGGGGCGCGGGGATTTGAACCCCGGTCCGCGGGTCTGGAGCCCG-3′. The three truncated mutants of the 3′-CCA end of *Tko* tRNA^{Trp} were prepared using the following primers (In all three reverse-primers, the first underlined nucleotide was methylated on its 2′-*O* ribose): Tk-TrpF, 5′-**GGGTAATACGACTCACTATA**GGGGGCGTGGTGTAGCCTGGTCCATCATCGCGCGGGCTCCAGACCCGCGG-3′; ΔA-R, 5′-G̲GTGGGGGCGCGGGGATTTGAACCCCGGTCCG̲CGGGTCTGGAGCCCG-3′; ΔCA-R, 5′-G̲TGGGGGCGCGGGGATTTGAACCCCGGTCCGCGḠGGTCTGGAGCCCG-3′; ΔCCA-R, 5′-TG̲ GGGGCGCGGGGATTTGAACCCCGGTCCGCGḠGGTCTGGAGCCCG-3′; ΔACCA-R, 5′-G̲GGGGCGCGGGGATTTGAACCCCGGTCCGCGGḠTCTGGAGCCCG-3′. All transcripts were purified through anion exchange chromatography using a HiTrap Q-sepharose column (GE healthcare). Mu-

tant (ΔA, ΔCA, ΔCCA and ΔACCA) RNA transcripts were further PAGE-purified using a 15% PAGE (7M Urea) gel (Supplementary Figures S8A and S8B).

Measurement of $_{Tko}$Trm11 activity

The enzymatic assay was measured by incorporation of ^{14}C-methyl groups from [methyl-^{14}C]-SAM onto the *Tko* tRNA^{Trp} transcript (Supplementary Figure S2A); 0.1 μM enzyme, 10 μM transcript and 11 μM [methyl-^{14}C]-SAM in 35 μl of buffer A (50 mM Tris-HCl (pH 7.5), 5 mM MgCl$_2$, 6 mM 2-mercaptoethanol and 50 mM KCl) were incubated for various times (0, 0.5, 2, 8, 16, 32 and 64 min) at 50°C. An aliquot (30 μl) was then used for the filter assay (Supplementary Figure S2B).

In order to discriminate the m^{2}G and m$^2_2$G formation activities of $_{Tko}$Trm11, we employed two-dimensional TLC (54). The ^{14}C-methylated RNA was dissolved in 5 μl of 50 mM ammonium acetate (pH 5.0) and digested with 2.5 units of nuclease P1, and then 2 μl of standard nucleotides containing 0.05 A$_{260}$ units each of pA, pG, pC and pU was added. A total of 2 μl of the sample was spotted onto a thin layer plate (Merck code number 1.05565, cellulose F) and separated using the following two solvent systems: Supplementary Figures S2C, S2D and S6B, first dimension, isobutyric acid/concentrated ammonia/water, 66:1:33, v/v; second dimension, isopropyl alcohol/HCl/water, 70:15:15, v/v; Supplementary Figure S2D, first dimension, isobutyric acid/concentrated ammonia/water, 66:1:33, v/v/v; second dimension, 0.1 M Sodium phosphate (pH 6.8), ammonium sulfate, n-propanol, 100:60:2, v/w/v. Incorporation of ^{14}C-methyl groups was monitored with a Fuji Photo Film BAS2000 imaging analyzer. Standard nucleotides were marked by UV 260 nm irradiation.

To visualize the methylation activity, we used 10% PAGE (7 M urea) and an imaging analyzer system. In brief, tRNA (0.1 A$_{260}$ units) was incubated with 0.1 μM $_{Tko}$Trm11 and 11 μM [methyl-^{14}C]-SAM for 10 min at 50°C in 35 μl of buffer A and then loaded onto a 10% polyacrylamide gel (7 M urea). The gel was stained with methylene blue and dried. The incorporation of ^{14}C-methyl groups into tRNA was monitored with an imaging analyzer as described above.

Measurements of kinetic parameters for SAM

We initially performed time course experiments at 50°C with 0.1 μM $_{Tko}$Trm11, 11 μM *Tko* tRNA^{Trp} transcript and 11 μM [methyl-^{14}C]-SAM in 200 μl of buffer A. The aliquots (30 μl each) were taken at appropriate times (0, 2, 5, 7.5, 10 and 15 min) and formations of ^{14}C-pm^{2}G and ^{14}C-pm$^2_2$G were monitored by two-dimensional TLC. Under these conditions, most of the pm^{2}G was observed at 10 min, and m$^2_2$G formation was undetectable by autoradiography (Supplementary Figure S6B). Kinetic parameters for SAM were determined by incorporation of ^{3}H-methyl groups from [methyl-^{3}H]-SAM into tRNA. The following conditions were used for the kinetics: 0.1 μM $_{Tko}$Trm11, 11 μM tRNA^{Trp} transcript and various concentrations (0.8, 1.5, 3.0, 6.0, 12.0, 24.0, 36.0, 48.0, 60.0 and 72.0 μM) of [methyl-^{3}H]-SAM were incubated at 50°C for 10 min, and then the filter assay was performed.

Table 1. Data collection and refinement statistics

	apo-$_{Tko}$Trm11	$_{Tko}$Trm11–SAM	SeMet I291M
Data collection			
Wavelength (Å)	1.0000	1.0000	0.9791
Space group	$P2_12_12_1$	$P2_12_12_1$	$P2_12_12_1$
Cell dimensions			
a, b, c (Å)	47.73, 53.52, 134.86	47.60, 53.79, 134,75	47.65, 53.81, 134,84
α, β, γ (°)	90, 90, 90	90, 90, 90	90, 90, 90
Resolution (Å)	50–1.70 (1.73–1.70)	50–1.74 (1.80–1.74)	50–1.75 (1.76–1.70)
R_{merge}[a]	5.1 (59.4)	4.3 (21.7)	10.1 (33.8)
$I / \sigma I$	53.7 (4.2)	41.6 (6.7)	106.7 (15.5)
Completeness (%)	99.8 (100.0)	99.7 (99.3)	100.0 (100.0)
Redundancy	7.1 (7.2)	5.1 (5.1)	29.0 (28.0)
Refinement			
Resolution (Å)	34.4-1.70	32.6-1.74	
No. reflections	34,442	35,857	
R_{work}[b] / R_{free}[c]	20.5/ 24.0	18.7/22.3	
No. atoms	2,774	2,909	
Protein	2,599	2,599	
Water	179	282	
SAM	0	1	
Avg. *B*-factors (Å^2)	25.9	18.8	
R.m.s. deviations			
Bond lengths (Å)	0.006	0.007	
Bond angles (°)	1.0	1.1	
Ramachandran plot (%)			
Most favored	92.8	92.0	
Additionally allowed	6.9	7.6	
Generously allowed	0.0	0.0	
Disallowed	0.4	0.4	

The value in the parentheses is for the highest resolution shell.

[a] $R_{merge} = \Sigma\Sigma_j |<I(h)> - I(h)_j|/\Sigma\Sigma_j <I(h)>|$, where $<I(h)>$ is the mean intensity of symmetry-equivalent reflections.

[b] $R_{work} = \Sigma (||F_p(obs) - F_p(calc)||)/\Sigma|F_p(obs)|$.

[c] $R_{free} = R$ factor for a selected subset (5%) of reflections that was not included in earlier refinement calculations.

Gel mobility shift assay

A gel mobility shift assay was carried out according to our previous reports (55). A total of 6.7 μM *Tko* tRNA^{Trp} transcript and various concentrations (0, 0.84, 1.68, 3.35 and 6.70 μM) of WT $_{Tko}$Trm11 or mutant were incubated in the buffer (50 mM Tris-HCl (pH 7.5), 5 mM MgCl$_2$, 6 mM β-mercaptoethonol and 50 mM KCl) at 60°C for 30 min. A 4x loading solution (0.25% bromphenol blue and 30% glycerol) was added to the each sample, and the mixtures were applied to a 6% polyacrylamide gel. After electrophoresis in running buffer (25 mM Tris-acetic acid (pH 7.0) and 5 mM Mg(OAc)$_2$) at 30 mA for 1 h, the gel was stained with Coomassie Brilliant Blue to detect protein and then with methylene blue to detect RNA.

Computer programs for figures

Structural figures were generated using PyMOL (DeLano Scientific, Palo Alto, CA, USA) and CueMol (http://www.cuemol.org). The electrostatic potential surface models were calculated using APBS (56). The schematic diagram of SAM interactions with the amino acid residues of $_{Tko}$Trm11 was generated using LIGPLOT (57). The amino acid sequence alignment was generated using ClustalW 1.83 (58) and ESPript (59) programs.

RESULTS AND DISCUSSION

Crystal structure determination

The $_{Tko}$Trm11 was cloned and overexpressed in *E. coli*, and the recombinant was purified using three chromatographic steps. The molecular weight of $_{Tko}$Trm11 is 39 255 Da, including the C-terminal His-tag and the protease cleavage site (^{332}LEVLFQGPSHHHHHH^{346}) (Supplementary Figure S1B). Seven grams of *E. coli* cells yielded ∼2 mg of purified $_{Tko}$Trm11. HRV-3C protease could cleave the C-terminal His-tag only partially, possibly because of steric hindrance between $_{Tko}$Trm11 and the HRV-3C protease. We confirmed that the purified $_{Tko}$Trm11 retained methylation activity (Supplementary Figure S2B). The first crystals of $_{Tko}$Trm11 appeared ∼6 months after we set up the initial crystallization screening. Upon optimization of the crystallization solution, crystals grew within 2 days. Crystals of apo-$_{Tko}$Trm11 and of $_{Tko}$Trm11 in complex with SAM diffracted to ∼1.7 Å resolution and belonged to the orthorhombic space group $P2_12_12_1$. For phasing using the Se-SAD method, we prepared Se-methionine labeled crystals. The initial electron density map allowed us to model one molecule of $_{Tko}$Trm11 in the asymmetric unit, consistent with the biological unit (i.e. hydrodynamic radius size estimate) observed with size exclusion chromatography (Supplementary Figure S1A). The structures of apo-$_{Tko}$Trm11 and $_{Tko}$Trm11–SAM were refined with reliable *R* and *R$_{free}$* factor values that validate the model (Table 1).
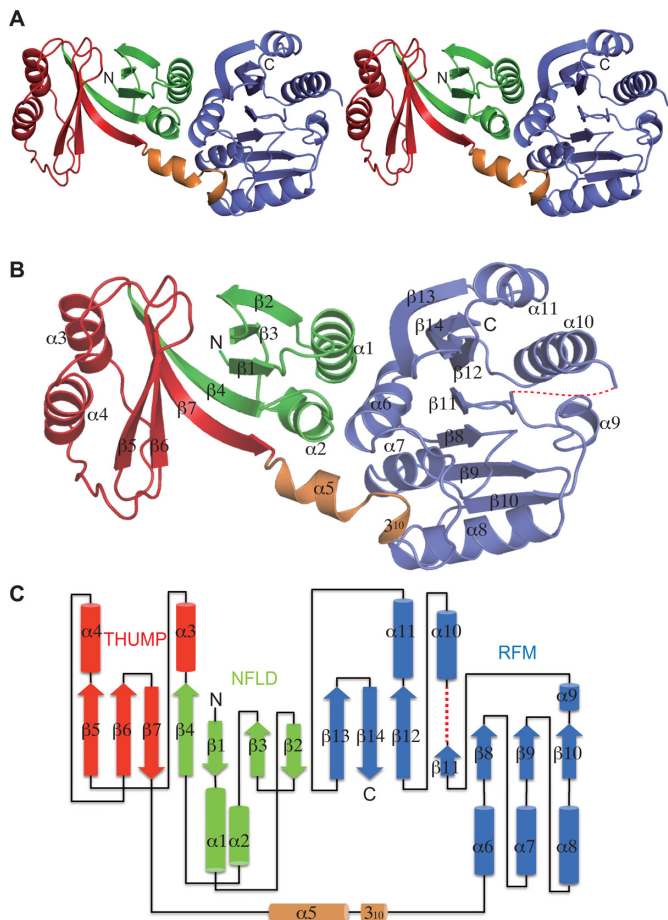
Figure 1. Crystal structure of aTrm11 from *Thermococcus kodakarensis*. (**A**) Ribbon stereo diagram of the overall structure. The three domains, NFLD (1–65 residues), THUMP domain (66–144 residues) and RFM domain (157–257 and 266–331 residues) are colored green, red, slate blue, respectively. A rigid linker region of the α- and 3_{10} helices (145–156 residues) is colored orange. The N and C-terminal ends are labeled as N and C, respectively. (**B**) Ribbon diagram of the overall structure. The secondary structures of the α helix, 3_{10} helix and β strand are labeled (in order) as the α 3_{10} and β, respectively. The dotted line (red color) indicates a disordered region (258–265 residues) (**C**) A $_{Tko}$Trm11 secondary structure topology diagram. The α helices and β strands are represented by cylinders and thick arrows, respectively. The dotted line (red color) indicates a disordered region (258–265 residues).

Overall structure

The overall shape of $_{Tko}$Trm11 is like a cylinder with approximate $60 \times 30 \times 30$ Å^3 dimensions (Figure 1A). The structure of $_{Tko}$Trm11 is comprised of three domains: NFLD (green), THUMP (red) and RFM (slate blue). The THUMP domain is connected to the C-terminal RFM domain via a rigid linker region (orange) consisting of two secondary structures, an α-helix joined to a more C-terminal 3_{10}-helix (Figure 1B and C). NFLD has been regarded as a minimal core of the THUMP domain (38). The entirety of NFLD and THUMP domains employs a globular α/β structure consisting of seven β strands and four α helices. The four β strands (β1–β4) of NFLD form one antiparallel β sheet together with two α helices (α1 and α2). In contrast to the structural arrangement of NFLD, the three β strands (β5–

β7) of THUMP domain form one mixed antiparallel and parallel β sheet together with two α helices (α3 and α4). The two β sheets are connected by two long kinked β strands (β4 and β7). Therefore, seven β strands (β1–β7) seem to form one twisted β sheet in the center of two domains, and the β sheet is packed by two α helices. On the other hands, the C-terminal RFM domain of $_{Tko}$Trm11 is a class I type of MTase that consists of seven β strands (β8–β14) and six α helices (α6–α11) (11). The parallel β sheet, forming by seven β strands (β8–β14), is sandwiched by the three α helices out of six α helices (α6–α11), indicating that the architecture of the RFM domain in $_{Tko}$Trm11 is a classical feature that belongs to the RFM superfamily and present in other MTases. The entire region comprising the NFLD and THUMP domains is reported to function as the tRNA-binding module in other tRNA modifying-enzymes (33). Our structure-based sequence alignment analysis suggests that the structural arrangement of $_{Tko}$Trm11 is conserved in aTrm11 from the *Pyrococcus* genus, which are species related to *Tko* (Supplementary Figure S3). Thus, $_{Tko}$Trm11 probably possess the ability to specifically recognize the tRNA substrate, similar to the substrate recognition mechanism of aTrm11 from *Pyrococcus* species as previously reported (34,36).

Structural comparison

Our structural analysis provided a detailed configuration of $_{Tko}$Trm11. To estimate the functional features of $_{Tko}$Trm11 from its structural conservation, we searched for homologous structures using the DALI server (60). The most similar structure identified (i.e. the structure with the highest Z-score), was archaeal Trm14 from *Pyrococcus furiosus* (*Pfu*) (Figure 2A and B), which catalyzes the formation of m^{2}G6 in archaeal tRNA species (27). Furthermore, the structure of NFLD and THUMP domain in $_{Tko}$Trm11 is homologous to that of the NFLD and THUMP domain in other two tRNA-modifying enzymes ThiI (38) and CDAT8 (37). Their domains are shown to be responsible for tRNA recognition. The $_{Tko}$Trm11 and $_{Pfu}$Trm14 conformations of respective NFLD-THUMP and RFM domains superimposed well (Figure 2C and D), with root mean square deviations (r.m.s.d) of 2.7 Å and 3.0 Å that were estimated using their 136 and 205 Cα atoms. This high level of structural conservation between these regions suggests that $_{Tko}$Trm11 and $_{Pfu}$Trm14 (Supplementary Figure S4) are derived from a common ancestor. Importantly, however, the linker regions connecting the NFLD and RFM domains are not conserved between $_{Tko}$Trm11 and $_{Pfu}$Trm14. The $_{Tko}$Trm11 α- and 3_{10} helices linker is rather a flexible loop in $_{Pfu}$Trm14. Furthermore, the conformational location of the RFM domain is remarkably different between $_{Tko}$Trm11 and $_{Pfu}$Trm14 (Figure 2E and F) when their NFLD-THUMP domain is superimposed. The RFM domain of $_{pfu}$Trm14 is largely rotated and shifted more upward and closer to the NFLD-THUMP domain than it is in the $_{Tko}$Trm11 structure. The movement of the RFM domain in $_{Tko}$Trm11 seems to be restricted because of the rigidness (i.e. like a tension-rod) of the linker region formed by the α- and 3_{10} helices. However, the RFM domain of $_{Pfu}$Trm14 can be more flexible than that of $_{Tko}$Trm11 because the linker region consists of loop structure. Thus, we
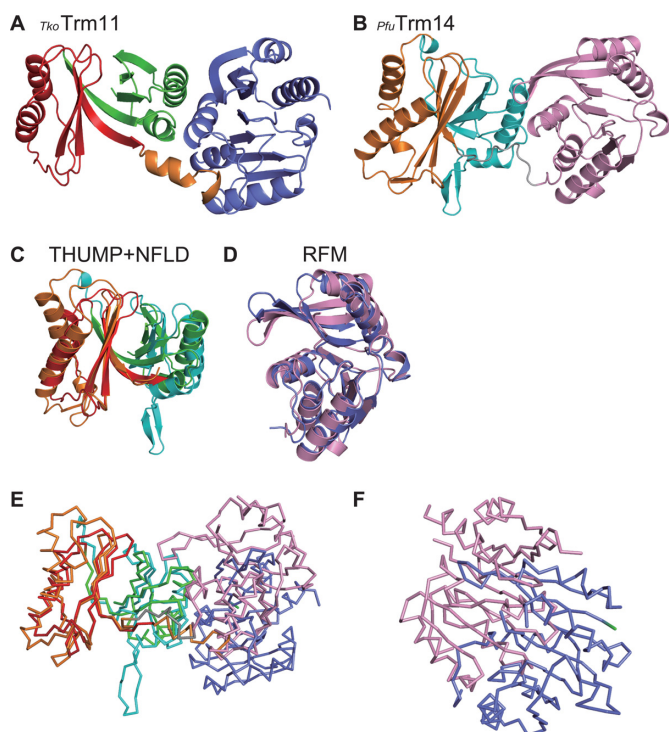
Figure 2. Structural comparison of $_{Tko}$Trm11 and $_{Pfu}$Trm14 (PDB ID = 3TLJ). (**A**) Ribbon diagram of the overall structure of $_{Tko}$Trm11. The three domains, NFLD, THUMP and RFM, and the rigid linker region are colored as in Figure 1A. (**B**) Ribbon diagram of the overall structure of $_{Pfu}$Trm14. The three domains, NFLD, THUMP and RFM, and a loop linker are colored cyan, orange, pink and grey, respectively. (**C**) Superimposition (obtaining by aligning respective Cα atoms) of the THUMP (red) and NFLD (green) domains of the $_{Tko}$Trm11 structure onto that of the THUMP (orange) and NFLD (cyan) domains of the $_{Pfu}$Trm14 structure. (**D**) Superimposition (obtaining by aligning respective Cα atoms) of the $_{Tko}$Trm11 RFM (slate blue) domain onto that of the $_{Pfu}$Trm14 RFM (pink) domain. (**E**) Line diagram of the overall structure based on the superimposed Cα atoms of THUMP and NFLD domains between the $_{Tko}$Trm11 and $_{Pfu}$Trm14 structures. (**F**) Close-up view of the structural deviation of RFM domains ($_{Tko}$Trm11, slate blue and $_{Pfu}$Trm14, pink) based on the superimposed Cα atoms of THUMP and NFLD domains between the $_{Tko}$Trm11 and $_{Pfu}$Trm14 structures.

infer that the structural difference of linker regions between $_{Tko}$Trm11 and $_{Pfu}$Trm14 attributes to the difference in spatial location of the RFM domain. Because the RFM domain includes a catalytic center, the distinct linker-regions might have an effect on the site specificity of the two enzymes.

The SAM-binding mode

To examine how the SAM binds to the catalytic domain of RFM in $_{Tko}$Trm11, we determined the X-ray crystal structure of the $_{Tko}$Trm11–SAM complex at 1.74 Å resolution. One SAM molecule was bound to the pocket of the RFM domain (Figure 3A). The SAM-binding pocket is composed of several residues, which are conserved in archaeal Trm11 enzymes (Supplementary Figures S5A and S5B). The eight residues (I163, D185, F187, D208, I209, R210, D235 and D254) that interact with the SAM molecule are illustrated in Figure 3B. These residues belong to the conserved motifs I,
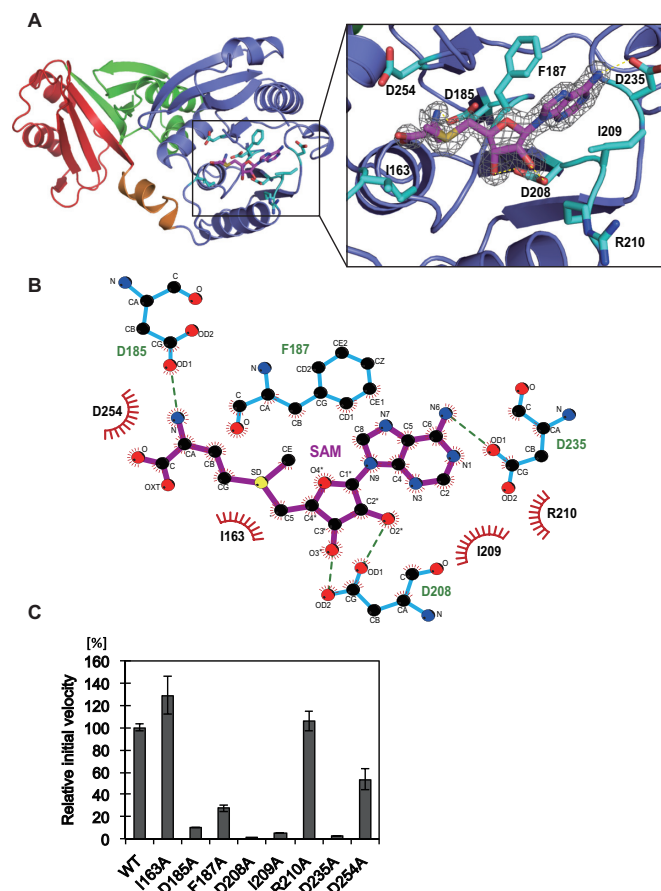

Figure 3. The SAM-binding site of $_{Tko}$Trm11 in complex with SAM. (**A**) Close-up view of the SAM molecule and its binding residues illustrated as stick models (magenta and cyan, respectively). Electron density map around the SAM molecule contoured at 2.0 σ. (**B**) Ligplot diagram (64) of interactions between $_{Tko}$Trm11 amino acid residues and the bound SAM molecule. (**C**) Methyl transfer activity of the alanine-substituted mutant proteins. The mutant name indicates the site of alanine substitution. The initial velocity of wild-type (WT) $_{Tko}$Trm11 is expressed as 100%. Error-bar indicates the SD (standard deviation) that was calculated between three independent experiments.

II, III and IV that exist in SAM dependent MTases (Supplementary Figure S3) (25,61,62). The three aspartate residues at amino acid numbers 185, 208 and 235, are included in conserved motifs I, II and III, respectively, and form four hydrogen bonds with the SAM molecule. As it has been predicted by bioinformatics studies of $_{Pab}$Trm11 (28), the three aspartates indeed coordinate the methionine moiety, the 2′- and 3′- hydroxyl groups of the ribose moiety, and the N^6 atom of the adenine moiety, respectively. On the other hands, the adenine moiety of the SAM molecule is specifically recognized by two hydrophobic residues (F187 and I209), resulting in the formation of stacking interactions between the two residues and the adenine moiety. Other $_{Tko}$Trm11 residues contribute several van der Waals contacts with the SAM molecule. The bound SAM molecule is structurally extended, and its conformation is very similar to that of the SAM molecule in complex with $_{Pfu}$Trm14 (27).

To determine whether the side chain of these residues plays an important role in the binding of the SAM molecule to $_{Tko}$Trm11, we performed an alanine-scanning mutagenesis study. The initial velocities of six mutants (D185A, D208A, I209A, R210A, D235A and D254A: Supplementary Figure S6A) showed a decrease compared to that of the WT enzyme. Specifically, the initial velocities of D185A, F187A, D208A, I209A and D235 were less than 20% of that of WT, suggesting that the formations of hydrogen bonds and hydrophobic interactions between those residues and the SAM molecule are required for the binding of SAM into the pocket of the RFM domain. A kinetic study further confirmed the enzymatic significance of these SAM-binding residues (Table 2). In this study, we optimized the reaction time and conditions for the measurement of the first $_{Tko}$Trm11 methyl transferase reaction (m^{2}G formation) at the position G10 of *Tko* tRNA^{Trp} (see Materials and Methods). The mono-methylation was confirmed by TLC (Supplementary Figure S6B). The four mutants, F187A, I209A, D235A and D254A, had respective apparent K_m values of 23, 23, 45 and 26 μM, which are 3.2–6.4 times higher than that of the WT enzyme, and the apparent K_m value of D208A was more than 1200 μM. These results indicate the large effect that these residues contribute to the binding affinity of $_{Tko}$Trm11 for the SAM molecule, and thereby leading to the decrease of V_{max} values in the mutants. Because the V_{max}/K_m values of D208A and D235A mutant are less than 0.00039 and 0.02, respectively, each of their three hydrogen bonds with SAM (D208 Oδ1—ribose 2′O, D208 Oδ2—ribose 3′O and D235 Oδ1—SAM N^6) seems to be the most important for SAM-recognition compared to other interactions, which are the hydrophobic interactions between two residues (F187 and I209) and the adenine moiety of SAM molecule, and the van der Waals contacts formed by the D254 and $\alpha-NH_3^+$ and α-COO$^-$ group of SAM molecule. Although the V_{max} value of D185A was decreased to 230 nmol mg^{-1} h^{-1}, which is 3.2 times lower than that of the WT enzyme, the K_m value was almost the same as that of the WT enzyme. The decrease is probably due to the disruption of the D185 Oδ1—SAM $\alpha-NH_3^+$ hydrogen bond. The formed hydrogen bond determines the spatial location of the $\alpha-NH_3^+$ and α-COO$^-$ groups of the SAM molecule, resulting in the stabilization of the entire SAM molecule. The amino-carboxyl group of SAM molecule is often shown to be a disordered region in other tRNA MTases because no residues are observed directly interacting with a SAM molecule. Therefore, $_{Tko}$Trm11 D185 might contribute to the transfer speed of the SAM methyl group to N^2-guanine and/or the release speed of product *S*-adenosyl-L-homocystein from the pocket of the $_{Tko}$Trm11 RFM domain. Other region ($_{Tko}$Trm11 residues 258–265), which is closely located near the SAM-binding pocket, was unable to be modeled in our structure due to missing electron density. This region is a C-terminal conserved catalytic motif IV (^{254}DPPY^{257}) (Supplementary Figure S3), which is involved in the catalytic reaction and recognition of a guanine moiety (28). The residues in motif IV are also found in $_{pfu}$Trm14 (^{293}NLPY^{296}) and in *Thermus thermophilus* RsmC (^{305}NPPF^{308}), which is a SAM dependent 16S rRNA (m^{2}G1207) methyltransferase (63). In the crys-
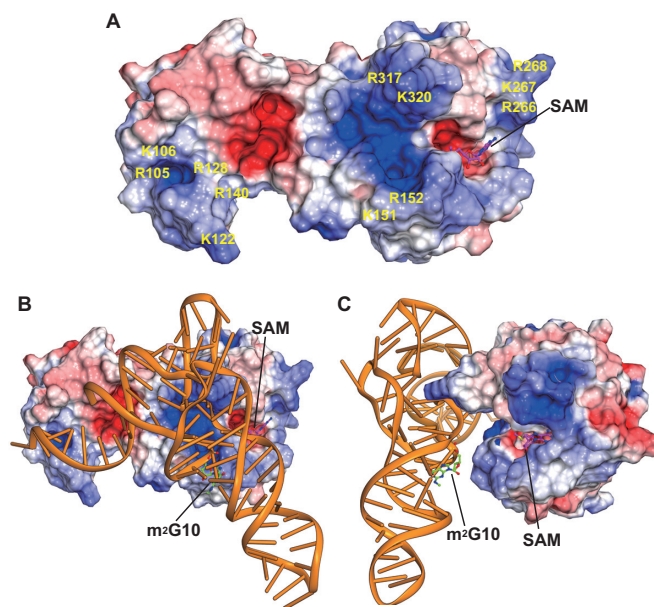

Figure 4. Search for the tRNA recognition site of $_{Tko}$Trm11. (**A**) Surface model of $_{Tko}$Trm11 colored according to electrostatic potential represented as a gradient from negative (red) to positive (blue). The positions of positively charged residues are labeled on the surface model. The stick model represents the SAM molecule bound to $_{Tko}$Trm11. (**B**) Proposed model of the complex formed between $_{Tko}$Trm11 and yeast tRNA^{Phe} with SAM (magenta) and m^{2}G10 (green) illustrated as stick representations. (**C**) Figure 4B rotated 90° clockwise around its vertical axis.

tal structure of RsmC in complex with SAM and guanosine molecules, the aromatic ring of F308 forms a stacking interaction with a substrate guanine moiety that is flipped out from the rRNA. Among the three enzymes, their SAM-binding mode and motif IV are structurally conserved. Therefore, it is likely that Y257 of $_{Tko}$Trm11 as well as Y296 of $_{pfu}$Trm14 provide almost the same hydrophobic interaction for the substrate base as does F308 of *T. thermophilus* RsmC. However, the underlying mechanism by which the $_{Tko}$Trm11 produces not only a N^2-methylguanosine (m^{2}G) but also a N^2, N^2-dimethylguanosine (m$^2_2$G) remains a puzzling question despite of the structural conservation of catalytic center of three enzymes. An observation of structural intermediate methylated by $_{Tko}$Trm11 could be needed to answer the question, although U25 and a V-loop of four nucleotides of yeast tRNA^{Phe} might be major determinants for the formation of m$^2_2$G as previously reported (36).

Recognition of tRNA by $_{Tko}$Trm11

We calculated an electrostatic potential map of the $_{Tko}$Trm11–SAM complex structure (Figure 4A) in order to examine specific residues responsible for the recognition of substrate tRNA. As a result, many positively charged residues are observed on the surface areas of $_{Tko}$Trm11 located on the THUMP domain, linker region and RFM domains, suggesting that the positively charged residues are probably involved in the recognition of tRNA. Extensive biochemical studies have reported that the structural elements of acceptor stem, T-arm and V-loop in the *S. cerevisiae* tRNA^{Phe} and tRNA^{Asp} species are important for the

Table 2. Kinetic parameters for SAM

Sample names	$K_m \mu M$	$V_{max} nmol\, mg^{-1}\, h^{-1}$	$k_{cat} min^{-1}$	Relative V_{max}/K_m
WT	7 ± 1	746 ± 46	0.49 ± 0.08	1.00
D185A	6 ± 1	230 ± 18	0.15 ± 0.03	0.34
F187A	23 ± 1	319 ± 21	0.21 ± 0.02	0.13
D208A	>1200	$10 - 50$	$0.007 - 0.03$	<0.00039
I209A	23 ± 1	309 ± 31	0.20 ± 0.04	0.12
D235A	45 ± 3	111 ± 11	0.07 ± 0.03	0.02
D254A	26 ± 3	154 ± 9	0.10 ± 0.02	0.05

The K_m/V_{max} value is expressed relative to that of the wild type enzyme, which is set to 1.00.

substrate specificity and formation of m$^2_2$G by the $_{pab}$Trm11 (34,36). Based on the previous results for the substrate recognition and our above finding of the positive surface areas of $_{Tko}$Trm11, the docking model of $_{Tko}$Trm11 in complex with *S. cerevisiae* tRNA^{Phe} was manually built (Figure 4B and C). Furthermore, the structure of the bacterial ThiI–RNA complex, which was reported recently (43), greatly contributed to the construction of its docking model. The docking model of the $_{Tko}$Trm11–tRNA^{Phe} complex shows that four structural components (a 3′-ACCA end, acceptor stem, T-stem and V-loop) interact with the THUMP-RFM domains and linker region of $_{Tko}$Trm11 along the positive surface areas. In addition, m^{2}G10 is located at the front of the SAM binding pocket, where the recognition and methylation for substrate N^2-guanosine can occur by the flipping out of the substrate tRNA G10 guanine moiety coinciding with the conformational changes of $_{Tko}$Trm11. Thus, these observations suggest that the positively charged residues, which are estimated by the electrostatic potential, may play a significant role as the tRNA-binding sites.

To clarify whether the Arg and Lys residues observed above are responsible for recognition of a substrate tRNA, we conducted a mutagenesis study: The positively charged $_{Tko}$Trm11 residues were each replaced with an alanine residue (Ala), which we expected to moderately disrupt interactions with the negative charges of tRNA generated by its phosphate backbone. Eighteen mutant proteins (R105A, K106A, R105A/K106A, K122A, R128A, R140A, K122A/R140A, K122A/R128A/R140A, K151A, R152A, K151A/R152A, R266A, K267A, R268A, R266A/K267A/R268A, R317A, K320A and R317A/K320A) were constructed and then purified (Supplementary Figures S6A, S6C and S6D). Figure 5A shows the relative velocities of WT $_{Tko}$Trm11 and of the 18 mutants. No significant changes in the initial velocities were observed in single mutants, but the double mutant (K151A/R152A) showed a ∼30% reduction in the initial velocity as compared to WT $_{Tko}$Trm11 (Figure 5A). The K151A and R152A residues are located in the linker region connecting the THUMP and RFM domains, likely interacting with the phosphate backbone around the acceptor stem of tRNA in our docking model of $_{Tko}$Trm11–tRNA (Figure 4B and C). We hypothesized that the double mutant, K151A/R152A, might have a synergistic effect on the binding affinity for tRNA as compared to the single mutants. We therefore tested its ability to bind tRNA in a gel shift assay (Figure 5B, C and D). As a result, one band that corresponds to the formation of a complex between WT $_{Tko}$Trm11 and tRNA^{Trp} was detected after an increase
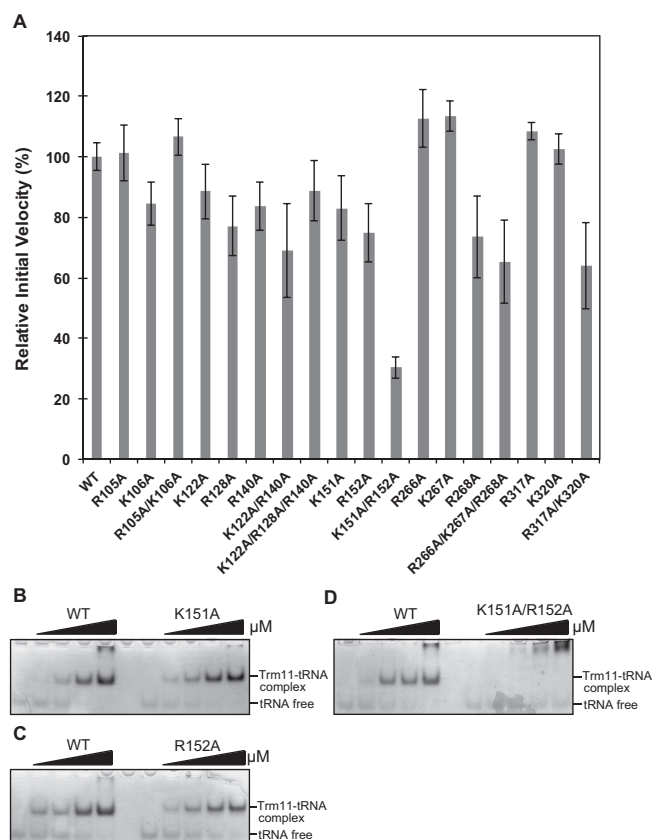

Figure 5. Putative tRNA-binding sites. (**A**) Methyl transfer activity of the alanine-substituted mutant proteins. The mutant name indicates the site of alanine substitution. The initial velocity of WT $_{Tko}$Trm11 is expressed as 100%. Error-bar indicates the standard deviation (SD) that was calculated between three independent experiments. (**B**) The binding-affinity values of the WT $_{Tko}$Trm11 and K151A mutant for *Tko* tRNA^{Trp} were analyzed by a gel mobility shift assay. (**C**) The binding-affinity values of WT $_{Tko}$Trm11 and R152A mutant for *Tko* tRNA^{Trp} were also analyzed by a gel mobility shift assay. (**D**) The binding-affinity values of WT $_{Tko}$Trm11 and K151A/R152A mutant for *Tko* tRNA^{Trp} were analyzed by a gel mobility shift assay. The formations of a complex by WT $_{Tko}$Trm11 or each of the three mutants with *Tko* tRNA^{Trp} and unbound free tRNA were indicated by two black lines labeled on the right side of the gel.

in the concentration of WT $_{Tko}$Trm11. The free tRNA^{Trp} gradually disappeared with the increasing concentration of WT $_{Tko}$Trm11. Similar results were obtained for the two single mutants (K151A and R152A). In contrast to these findings about WT$_{Tko}$Trm11 and the two single mutants, formation of a complex between K151A/R152A

and tRNA[Trp] was not observed (Figure 5D) despite having ∼30% relative activity as compared to WT *Tko*Trm11, and there remained free tRNA[Trp] that was not bound to the double mutant. These results suggest that K151 and R152 residues synergistically contribute to the recognition of a substrate tRNA. Similarly, the R266, K267, R268, R317 and K320 residues can contribute to tRNA-binding because the corresponding double and triple mutants (R266A/K267/R268A and R317A/K320A) showed a decrease in a nearly 50% decrease in initial velocities in comparison with the relevant single mutants (R266A, K267A, R268A, R317A and K320A). The R317 and K320 residues in the RFM domain seem to recognize the V-loop of tRNA (Figure 4B). In the case of three R266, K267 and R268 residues, it is difficult to find an interaction between the three residues and tRNA without a conformational change of the docking model. Taken together, our data suggest that these positively charged residues distributed in the linker region and RFM domain play a significant role as the tRNA-binding sites.

Possible mechanism for site specificity

As we described above, there is a striking structural similarity between the NFLD and THUMP domains among tRNA modifying-enzymes, *Tko*Trm11, *Pfu*Trm14, ThiI and CDAT8. ThiI is a 4-thiouridine synthetase that catalyzes the formation of 4-thiouridine at position 8 ($_s$4U8) in bacterial and archaeal tRNA species. Recently, the X-ray crystal structure of *Thermotoga maritime* (*Tma*) ThiI in complex with truncated tRNA has been determined (43) and has revealed that the RNA is mainly bound to the NFLD and THUMP domains of one subunit within the homodimer of ThiI thereby positioning U8 close to the pyrophosphatase domain (PPase) active site in the other subunit (Figure 6A). To examine the difference of RNA-binding mode between the *Tma*ThiI–RNA complex and docking model of *Tko*Trm11–tRNA[Phe] complex (Figure 4B and C), we superimposed it onto the *Tma*ThiI–RNA complex by aligning their respective main chain Cα atoms of their NFLD and THUMP domains (Figure 6B). These two domains superimpose well between both enzymes with a r.m.s.d value of 3.2 Å. Remarkably, the structural orientation of the RNA molecule in our docking-model of *Tko*Trm11–tRNA[phe] is similar to that of the truncated RNA molecule in the *Tma*ThiI–RNA complex structure. The accepter stem in tRNA is a structural element important for the recognition of substrate tRNA in the both enzymes. It has previously been demonstrated that the 3′-ACCA end of tRNA[Phe] is essential for the C4-thiolation of U8 (42). In fact, the crystal structure of the *Tma*ThiI–RNA complex reveals that the THUMP domain specifically recognizes the 3′-ACCA end, suggesting a molecular ruler that defines the length from the 3′-ACCA end to the modification site ((43), Figure 6B). The 3′-CCA end is bound into a groove of the THUMP domain, which is composed of the β5-strand (T102-K109), the α4-helix (V118-N132) and CCA-binding loop (F133-D144; Supplementary Figure S7). This groove in the THUMP domain of *Tma*ThiI is structurally homologous to a THUMP domain groove in *Tko*Trm11 formed by the β5-strand (A85-T92), the α4-helix (V100-H112) and
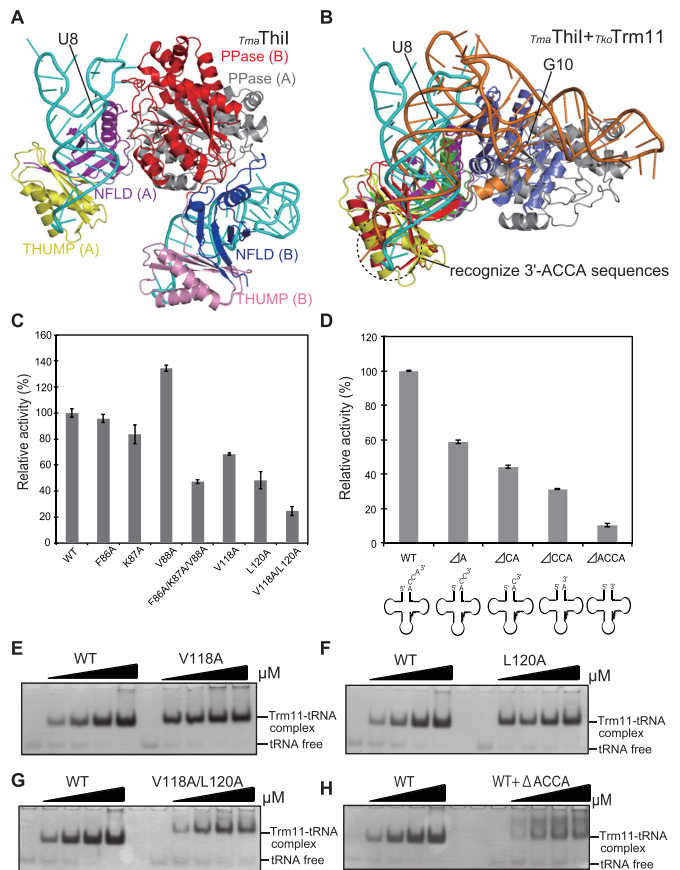

Figure 6. *Tko*Trm11 specifically recognizes the 3′-ACCA end of tRNA through the THUMP domain common to other tRNA-modifying enzymes, *Tma*ThiI, *Pfu*Trm14 and CDAT8. (**A**) Ribbon diagram of crystal structure of dimeric *Tma*ThiI in complex with truncated tRNA (PDB code, 4KR6). The THUMP, NFLD, PPase domains and truncated tRNA in the A-form structure are colored yellow, purple, gray and cyan, respectively. The THUMP, NFLD, PPase domains and truncated tRNA in the B-form structure are colored pink, blue, red and cyan, respectively. (**B**) Ribbon diagram of the *Tko*Trm11–tRNA complex model and the A-form of the *Tma*ThiI–RNA complex structure based on the superimposed Cα atoms of the THUMP (red) and NFLD (green) domains of *Tko*Trm11 onto that of the THUMP (yellow) and NFLD (purple) domains of the *Tma*ThiI structure (A-form). The tRNA of the *Tko*Trm11–tRNA complex model and RNA of *Tma*ThiI–RNA complex are colored orange and cyan, respectively. (**C**) Methyl transfer activity of the alanine-substituted mutant proteins. The mutant name indicates the site of alanine substitution. The initial velocity of wild-type *Tko*Trm11 is expressed as 100%. Error-bar indicates the SD (standard deviation) that was calculated between three independent experiments. (**D**) Relative activity of methylation by *Tko*Trm11 with the 3′-terminal truncated *Thermococcus kodakarensis* tRNA[Trp] (full-length 76 mer) mutants, ΔA (76A is truncated), ΔCA (76A and 75C are truncated), ΔCCA (76A, 75C and 74C are truncated) and ΔACCA (76A, 75C, 74C and 73A are truncated). The specific activity of WT *Tko*Trm11 is expressed as 100%. Error-bar indicates the SD that was calculated between three independent experiments. (**E**) The binding-affinity values of WT *Tko*Trm11 and V118A mutant for *Tko* tRNA[Trp] analyzed by the gel mobility shift assay. (**F**) The binding-affinity values of WT *Tko*Trm11 and L120A mutant for *Tko* tRNA[Trp] analyzed by the gel mobility shift assay. (**G**) The binding-affinity values of WT *Tko*Trm11 and V118A/L120A mutant for *Tko* tRNA[Trp] analyzed by the gel mobility shift assay. (**H**) The binding-affinity values of WT *Tko*Trm11 for *Tko* tRNA[Trp] and ΔACCA analyzed by the gel mobility shift assay. The formations of a complex by WT *Tko*Trm11 or each of the three mutants with *Tko* tRNA[Trp] or ΔACCA and unbound free tRNA are indicated by two black lines labeled on the right side of the gel.

CCA-binding loop (A113-D124), although the residues of the groove appear to be slightly diversified between $_{Tma}$ThiI and $_{Tko}$Trm11. Therefore, $_{Tko}$Trm11 likely recognizes the 3′-ACCA end with site specificity like $_{Tma}$ThiI. To confirm this possibility, we selected five conserved residues (F86, K87, V88, V118 and L120) responsible for recognition of the 3′-ACCA end, followed by a mutagenesis study using the seven alanine-substituted mutants prepared (F86A, K87A, V88A, F86A/K87A/V88A, V118A, L120A and V118A/L120A; Supplementary Figure S6D). As shown in Figure 6C, the methylation activity of the two single mutants (F86A and K87A) was not significantly changed compared to that of WT $_{Tko}$Trm11, except for the V88A mutant with an increased relative activity. The V118A and L120A mutants showed 50–70% reduction in relative activity compared to WT $_{Tko}$Trm11. In the F86A/K87A/V88A and V118A/L120A mutants, the methylation activities were remarkably reduced, especially in the latter, with a decrease of ∼30% relative activity. We further performed a gel mobility shift assay to test the binding affinity of V118A/L120A to *Tko* tRNA^{Trp}. The amount of V118A/L120A–tRNA complex formation was considerably less than that of WT $_{Tko}$Trm11–RNA, V118A-tRNA and L120A–tRNA complex formation (Figure 6E, F and G). Unbound, free tRNA was still detected in the gel for the V118A/L120A mutant, although the molecular mixing ratio between V118A/L120A and tRNA was 1:1. These results indicate that the seven conserved residues synergistically contribute to recognition of the 3′-ACCA end. In the crystal structure of the $_{Tma}$ThiI–RNA complex, various interactions (i.e. polar contact, hydrogen bond formation and van der Waals contact), except electrostatic ones, between the groove of the THUMP domain and the 3′-ACCA end were shown to be responsible for recognition of the 3′-CCA end. Probably, such interactions occur in the groove of the THUMP domain of $_{Tko}$Trm11. We performed a mutational analysis for four *Tko* tRNA^{Trp} mutants (ΔA, ΔCA, ΔCCA and ΔACCA), in which the 3′-ACCA sequences of *Tko* tRNA^{Trp} were truncated one by one from the 3′ terminus of adenosine (Supplementary Figure S8A and B). Using purified wild-type (WT) *Tko* tRNA^{Trp} and its four mutants, their specific activities were measured at various times (Supplementary Figure S8C), and their relative activities at 8 min were further compared, as shown in Figure 6D. All mutants showed decreased activity compared to WT tRNA^{Trp}. The relative activities of ΔA, ΔCA, ΔCCA and ΔACCA mutants were gradually reduced to ∼60%, 50%, 30% and 10%, respectively, according to the deletion of one nucleotide from the 3′ terminus of *Tko* tRNA^{Trp}. Furthermore, we performed a gel mobility shift assay to confirm the binding affinity between WT $_{Tko}$Trm11 and ΔACCA mutant (Figure 6H). The formation of WT $_{Tko}$Trm11–ΔACCA complex yielded smeared bands, which reflected low binding affinity, compared to the formation of Wt $_{Tko}$Trm11–tRNA complex. These results clearly demonstrate that the 3′-ACCA end is required for the total activity of $_{Tko}$Trm11. However, the amplitude of decreased methylation activity in the ΔACCA mutant was rather low as compared to that observed for *E.coli* ThiI having <0.1% activity (42). In the case of ThiI, only the N-terminal THUMP-NFLD domain appeared to function as a tRNA-binding site, which could
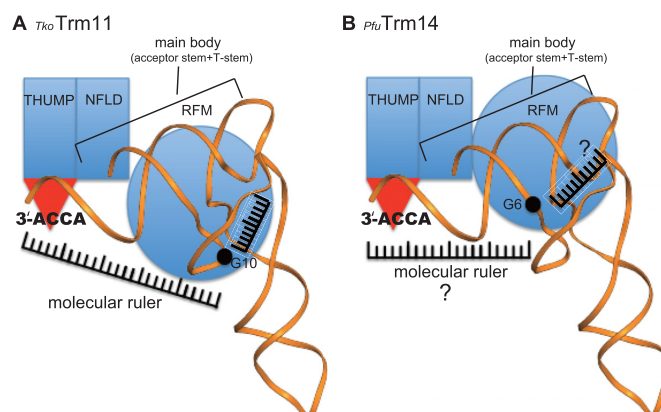

Figure 7. Cartoon diagram of the proposed tRNA recognition mechanism of (**A**) $_{Tko}$Trm11 and (**B**) $_{Pfu}$Trm14.

recognize not only the 3′-CCA end, but also the acceptor and T-stems (41,43). Free PPase domain of ThiI was unable to bind substrate tRNA. In contrast, the THUMP-NFLD domain of $_{Pab}$Trm11 showed rather low binding affinity to substrate tRNA (34), although we could not detect the formation of THUMP-NFLD domain–tRNA complex in $_{Tko}$Trm11 (data not shown). Our mutational analyses described above showed that the linker region and RFM domain likely recognized substrate tRNA (Figure 4B and C). The formation of K151A/R152A–tRNA complex was not observed (Figure 5D), however, that of V118A/L120A–tRNA and WT $_{Tko}$Trm11–ΔACCA complexes was still detected (Figure 6G and H). These findings indicate that the tRNA-binding affinities of the linker region and RFM domain maybe higher than that of the THUMP-NFLD domain in $_{Tko}$Trm11. Accordingly, $_{Tko}$Trm11 can maintain ∼10% relative activity using the ΔACCA mutant because it possesses RNA-binding sites in the THUMP domain, as well as in the linker region and RFM domain.

Therefore, we hypothesize that $_{Tko}$Trm11 employs the following substrate recognition mechanism: specific binding of the 3′-ACCA end to the groove of the THUMP domain determines the length from the 3′-ACCA end to the methylation site at the catalytic center of the RFM domain, and recognition of V-loop by the RFM domain defines the length from the V-loop to the methylation site. The two molecular rulers would intersect at the methylation site, thereby defining the site specificity of $_{Tko}$Trm11 (Figure 7A). Notably, the molecular ruler mechanism could be conserved in archeal Trm14, because the enzyme contains the NFLD and THUMP domains, which are structurally similar to those of $_{Tko}$Trm11 and $_{Tma}$ThiI. In particular, the structural arrangement of $_{Pfu}$Trm14 is almost the same as that of $_{Tko}$Trm11. Furthermore, $_{Pfu}$Trm14 possesses a groove of the THUMP domain responsible for specific binding of the 3′-ACCA end, and the groove is composed of sequences similar to those of $_{Tko}$Trm11 and $_{Tma}$ThiI (Supplementary Figures S7 and S9A). The RFM domain of bacterial TrmN, which is almost identical to that of $_{Pfu}$Trm14, was shown to be responsible for the recognition of substrate tRNA (27). These observations indicate that $_{Pfu}$Trm14 probably employs the molecular ruler mecha-

nism common to $_{Tko}$Trm11. Nonetheless, the site specificity of $_{Pfu}$Trm14 is distinct from that of $_{Tko}$Trm11. Moreover, structural comparison of $_{Tko}$Trm11 and $_{Pfu}$Trm14 showed only two differences (Figure 2E, F and Supplementary Figure S9B): the linker region connecting the THUMP domain to the RFM domain; and the spatial location of the RFM domain, which might be caused by the difference in linker regions. We also found that the linker region of $_{Tko}$Trm11 contributes to the recognition of tRNA by electrostatic interactions between the positively charged residues and the negatively charged phosphate groups (Figures 4B and 5D). Thus, our results allow us to propose molecular ruler mechanism models for the site specificity of two tRNA MTases, $_{Tko}$Trm11 (Figure 7A) and $_{Pfu}$Trm14 (Figure 7B). The acceptor stem and T-stem play a significant role as the 'main body,' which is bound by the NFLD and THUMP domains, and thereby fixes the orientation of the stems as shown in the crystal structure of the $_{Tma}$ThiI–RNA complex and our docking model of the $_{Tko}$Trm11–tRNA^{Phe} complex (Figure 6A and B). The fixed orientation of acceptor stem and T-stem is probably a common feature of tRNA-modifying enzymes containing the NFLD and THUMP domains. The position of the catalytic center of the RFM domain in $_{Tko}$Trm11 is distinct in $_{Pfu}$Trm14 because of the structural difference in the linker regions of $_{Tko}$Trm11 and $_{Pfu}$Trm14. In $_{Tko}$Trm11, the K151 and R152 of the linker region appears to be involved in the recognition of tRNA (Figure 5D), and the R317 and K320 of the RFM domain may recognize the V-loop of the tRNA responsible for the formation of m$^2_2$G10. Therefore, the lengths from the 3′-ACCA end and the V-loop to the methylation site in $_{Tko}$Trm11 are likely to be different from those in $_{Pfu}$Trm14, although the existence of molecular ruler remains uncertain in the RFM domain of $_{Pfu}$Trm14 (Figure 7A and B). Indeed, the lengths of the molecular ruler may have an effect on the specific position of methylation, resulting in the difference in site specificity of $_{Tko}$Trm11 and $_{Pfu}$Trm14. In fact, $_{Tko}$Trm11 specifically transfers a methyl group to either N^2-guanosine or N^2-monoguanosine at position 10 in tRNA, while the formation of N^2-methylguanosine by $_{Pfu}$Trm14 is found at position 6. However, further structural determination of $_{Tko}$Trm11–tRNA and $_{Pfu}$Trm14–tRNA complexes will be needed to ensure the proposed molecular ruler mechanism models for site specificity of $_{Tko}$Trm11 and $_{Pfu}$Trm14.

In conclusion, we resolved the first X-ray crystal structure of $_{Tko}$Trm11, and our results reveal that it is composed of NFLD, THUMP and RFM domains, and that one linker region formed by both an α-helix and a 3$_{10}$ helix connects the THUMP and RFM domains. There is striking structural similarity between the NFLD and THUMP domains of the tRNA-modifying enzymes $_{Tko}$Trm11, $_{Pfu}$Trm14, $_{Tma}$ThiI and archeal CDAT8. The structural arrangement of $_{Tko}$Trm11 is almost the same as that of $_{Pfu}$Trm14, indicating that $_{Tko}$Trm11 and $_{Pfu}$Trm14 are derived from a common ancestor. However, each of the linker regions connecting the THUMP and RFM domains of these two tRNA MTases is distinct from the other. The linker region therefore appears to be involved in the specificity of methylation site of $_{Tko}$Trm11 and $_{Pfu}$Trm14. The structure of the $_{Tko}$Trm11–SAM complex showed that the SAM molecule is struc-

turally extended in the pocket of the RFM domain, similar to that of the $_{Pfu}$Trm14–SAM complex. Furthermore, kinetic analysis identified the most important residues for the recognition of the SAM molecule. Our plausible docking model of the $_{Tko}$Trm11–yeast tRNA^{Phe} complex, which is based on biochemical results and structural similarity to the NFLD and THUMP domains of the $_{Tma}$ThiI–RNA complex, allow us to hypothesize that $_{Tko}$Trm11 employs a molecular ruler mechanism by which specific binding of the 3′-ACCA end with the groove of the THUMP domain and recognition of the V-loop by the RFM domain define the lengths from the 3′-ACCA end and V-loop to the site of methylation. The intersection of two molecular rulers maybe a specific site for methylation. Moreover, the different lengths of molecular rulers between $_{Tko}$Trm11 and $_{Pfu}$Trm14, which is probably caused by differences in their linker regions connecting the THUMP and RFM domains, might determine the specific site for methylation. Thus, our findings here provide a unified interpretation of the molecular mechanism of site specificity of tRNA MTase that contains the NFLD and THUMP domains.

ACCESSION NUMBERS

The atomic coordinates and structure factors have been deposited in the Protein Data Bank, www.rcsb.org (PDB ID code 5E71, 5E72).

SUPPLEMENTARY DATA

Supplementary Data are available at NAR Online.

ACKNOWLEDGEMENTS

FUNDING

REFERENCES

1. Cantara,W.A., Crain,P.F., Rozenski,J., McCloskey,J.A., Harris,K.A., Zhang,X., Vendeix,F.A., Fabris,D. and Agris,P.F. (2011) The RNA Modification Database, RNAMDB: 2011 update. *Nucleic Acids Res.*, **39**, D195–D201.
2. Jühling,F., Mörl,M., Hartmann,R.K., Sprinzl,M., Stadler,P.F. and Pütz,J. (2009) tRNAdb 2009: compilation of tRNA sequences and tRNA genes. *Nucleic Acids Res.*, **37**, D159–D162.
3. Motorin,Y. (2015) RNA Modification. *eLS.*, doi:10.1002/9780470015902.a0000528.pub3.
4. Abbott,J.A., Francklyn,C.S. and Robey-Bond,S.M. (2014) Transfer RNA and human disease. *Front Genet.*, **5**, 158.
5. Torres,A.G., Batlle,E. and Ribas de Pouplana,L. (2014) Role of tRNA modifications in human diseases. *Trends Mol. Med.*, **20**, 306–314.
6. Hori,H. (2014) Methylated nucleosides in tRNA and tRNA methyltransferases. *Front Genet.*, **5**, 144.
7. Dennis,P.P. and Omer,A. (2005) Small non-coding RNAs in Archaea. *Curr. Opin. Microbiol.*, **8**, 685–694.
8. Machnicka,M.A., Milanowska,K., Osman Oglou,O., Purta,E., Kurkowska,M., Olchowik,A., Januszewski,W., Kalinowski,S., Dunin-Horkawicz,S., Rother,K.M. *et al.* (2013) MODOMICS: a database of RNA modification pathways–2013 update. *Nucleic Acids Res.*, **41**, D262–D267.
9. Czerwoniec,A., Kasprzak,J.M., Kaminska,K.H., Rother,K., Pruta,E. and Bujnick,J.M. (2009) Folds and functions of domains in RNA modification enzymes. In: Grosjean,H (ed). *DNA and RNA modification enzymes: Structure, mechanism, function and evolution*. Landes Bioscience, Austin, pp. 289–302.
10. Schubert,H.L., Blumenthal,R.M. and Cheng,X. (2003) Many paths to methyltransfer: a chronicle of convergence. *Trends Biochem. Sci.*, **28**, 329–335.
11. Anantharaman,V., Koonin,E.V. and Aravind,L. (2002) SPOUT: a class of methyltransferases that includes spoU and trmD RNA methylase superfamilies, and novel superfamilies of predicted prokaryotic RNA methylases. *J. Mol. Microbiol. Biotechnol.*, **4**, 71–75.
12. Urbonavicius,J., Skouloubris,S., Myllykallio,H. and Grosjean,H. (2005) Identification of a novel gene encoding a flavin-dependent tRNA:m5U methyltransferase in bacteria–evolutionary implications. *Nucleic Acids Res.*, **33**, 3955–3964.
13. Delk,A.S., Nagle,D.P., Rabinowitz,J.C. and Straub,K.M. (1979) The methylenetetrahydrofolate-mediated biosynthesis of ribothymidine in the transfer-RNA of Streptococcus faecalis: incorporation of hydrogen from solvent into the methyl moiety. *Biochem. Biophys. Res. Commun.*, **86**, 244–251.
14. Delk,A.S., Nagle,D.P. and Rabinowitz,J.C. (1980) Methylenetetrahydrofolate-dependent biosynthesis of ribothymidine in transfer RNA of Streptococcus faecalis. Evidence for reduction of the 1-carbon unit by FADH2. *J. Biol. Chem.*, **255**, 4387–4390.
15. Yamagami,R., Yamashita,K., Nishimasu,H., Tomikawa,C., Ochi,A., Iwashita,C., Hirata,A., Ishitani,R., Nureki,O. and Hori,H. (2012) The tRNA recognition mechanism of folate/FAD-dependent tRNA methyltransferase (TrmFO). *J. Biol. Chem.*, **287**, 42480–42494.
16. Hamdane,D., Argentini,M., Cornu,D., Golinelli-Pimpaneau,B. and Fontecave,M. (2012) FAD/folate-dependent tRNA methyltransferase: flavin as a new methyl-transfer agent. *J. Am. Chem. Soc.*, **134**, 19739–19745.
17. Hamdane,D., Guerineau,V., Un,S. and Golinelli-Pimpaneau,B. (2011) A catalytic intermediate and several flavin redox states stabilized by folate-dependent tRNA methyltransferase from *Bacillus subtilis*. *Biochemistry*, **50**, 5208–5219.
18. Hamdane,D., Argentini,M., Cornu,D., Myllykallio,H., Skouloubris,S., Hui-Bon-Hoa,G. and Golinelli-Pimpaneau,B. (2011) Insights into folate/FAD-dependent tRNA methyltransferase mechanism: role of two highly conserved cysteines in catalysis. *J. Biol. Chem.*, **286**, 36268–36280.
19. Nishimasu,H., Ishitani,R., Yamashita,K., Iwashita,C., Hirata,A., Hori,H. and Nureki,O. (2009) Atomic structure of a folate/FAD-dependent tRNA T54 methyltransferase. *Proc. Natl. Acad. Sci. U.S.A.*, **106**, 8180–8185.
20. Menezes,S., Gaston,K.W., Krivos,K.L., Apolinario,E.E., Reich,N.O., Sowers,K.R., Limbach,P.A. and Perona,J.J. (2011) Formation of m^{2}G6 in *Methanocaldococcus jannaschii* tRNA catalyzed by the novel methyltransferase Trm14. *Nucleic Acids Res.*, **39**, 7641–7655.
21. Roovers,M., Oudjama,Y., Fislage,M., Bujnicki,J.M., Versées,W. and Droogmans,L. (2012) The open reading frame TTC1157 of *Thermus thermophilus* HB27 encodes the methyltransferase forming N^2-methylguanosine at position 6 in tRNA. *RNA*, **18**, 815–824.
22. Awai,T., Kimura,S., Tomikawa,C., Ochi,A., Ihsanawati,Bessho, Y., Yokoyama,S., Ohno,S., Nishikawa,K., Yokogawa,T. *et al.* (2009) *Aquifex aeolicus* tRNA (N^2,N^2-guanine)-dimethyltransferase (Trm1) catalyzes transfer of methyl groups not only to guanine 26 but also to guanine 27 in tRNA. *J. Biol. Chem.*, **284**, 20467–20478.
23. Constantinesco,F., Benachenhou,N., Motorin,Y. and Grosjean,H. (1998) The tRNA(guanine-26,N^2-N^2) methyltransferase (Trm1) from the hyperthermophilic archaeon *Pyrococcus furiosus*: cloning, sequencing of the gene and its expression in Escherichia coli. *Nucleic Acids Res.*, **26**, 3753–3761.
24. Constantinesco,F., Motorin,Y. and Grosjean,H. (1999) Characterisation and enzymatic properties of tRNA(guanine 26, N^2, N^2)-dimethyltransferase (Trm1p) from *Pyrococcus furiosus*. *J. Mol. Biol.*, **291**, 375–392.
25. Ihsanawati,Nishimoto, M., Higashijima,K., Shirouzu,M., Grosjean,H., Bessho,Y. and Yokoyama,S. (2008) Crystal structure of tRNA N^2,N^2-guanosine dimethyltransferase Trm1 from *Pyrococcus horikoshii*. *J. Mol. Biol.*, **383**, 871–884.
26. Awai,T., Ochi,A., Ihsanawati,Sengoku, T., Hirata,A., Bessho,Y., Yokoyama,S. and Hori,H. (2011) Substrate tRNA recognition mechanism of a multisite-specific tRNA methyltransferase, *Aquifex aeolicus* Trm1, based on the X-ray crystal structure. *J. Biol. Chem.*, **286**, 35236–35246.
27. Fislage,M., Roovers,M., Tuszynska,I., Bujnicki,J.M., Droogmans,L. and Versées,W. (2012) Crystal structures of the tRNA:m^{2}G6 methyltransferase Trm14/TrmN from two domains of life. *Nucleic Acids Res.*, **40**, 5149–5161.
28. Armengaud,J., Urbonavicius,J., Fernandez,B., Chaussinand,G., Bujnicki,J.M. and Grosjean,H. (2004) N^2-methylation of guanosine at position 10 in tRNA is catalyzed by a THUMP domain-containing, S-adenosylmethionine-dependent methyltransferase, conserved in Archaea and Eukaryota. *J. Biol. Chem.*, **279**, 37142–37152.
29. Purushothaman,S.K., Bujnicki,J.M., Grosjean,H. and Lapeyre,B. (2005) Trm11p and Trm112p are both required for the formation of 2-methylguanosine at position 10 in yeast tRNA. *Mol. Cell. Biol.*, **25**, 4359–4370.
30. Okada,K., Muneyoshi,Y., Endo,Y. and Hori,H. (2009) Production of yeast (m2G10) methyltransferase (Trm11 and Trm112 complex) in a wheat germ cell-free translation system. *Nucleic Acids Symp. Ser (Oxf).*, 303–304.
31. Liger,D., Mora,L., Lazar,N., Figaro,S., Henri,J., Scrima,N., Buckingham,R.H., van Tilbeurgh,H., Heurgué-Hamard,V. and Graille,M. (2011) Mechanism of activation of methyltransferases involved in translation by the Trm112 'hub' protein. *Nucleic Acids Res.*, **39**, 6249–6259.
32. Mueller,E.G., Buck,C.J., Palenchar,P.M., Barnhart,L.E. and Paulson,J.L. (1998) Identification of a gene involved in the generation of 4-thiouridine in tRNA. *Nucleic Acids Res.*, **26**, 2606–2610.
33. Aravind,L. and Koonin,E.V. (2001) THUMP–a predicted RNA-binding domain shared by 4-thiouridine, pseudouridine synthases and RNA methylases. *Trends Biochem. Sci.*, **26**, 215–217.
34. Gabant,G., Auxilien,S., Tuszynska,I., Locard,M., Gajda,M.J., Chaussinand,G., Fernandez,B., Dedieu,A., Grosjean,H., Golinelli-Pimpaneau,B. *et al.* (2006) THUMP from archaeal tRNA:m$^2_2$G10 methyltransferase, a genuine autonomously folding domain. *Nucleic Acids Res.*, **34**, 2483–2494.
35. Renalier,M.H., Joseph,N., Gaspin,C., Thebault,P. and Mougin,A. (2005) The Cm56 tRNA modification in archaea is catalyzed either by a specific 2′-O-methylase, or a C/D sRNP. *RNA*, **11**, 1051–1063.
36. Urbonavicius,J., Armengaud,J. and Grosjean,H. (2006) Identity elements required for enzymatic formation of N^2,N^2-dimethylguanosine from N^2-monomethylated derivative and its possible role in avoiding alternative conformations in archaeal tRNA. *J. Mol. Biol.*, **357**, 387–399.
37. Randau,L., Stanley,B.J., Kohlway,A., Mechta,S., Xiong,Y. and Söll,D. (2009) A cytidine deaminase edits C to U in transfer RNAs in Archaea. *Science*, **324**, 657–659.

38. Waterman,D.G., Ortiz-Lombardía,M., Fogg,M.J., Koonin,E.V. and Antson,A.A. (2006) Crystal structure of *Bacillus anthracis* ThiI, a tRNA-modifying enzyme containing the predicted RNA-binding THUMP domain. *J. Mol. Biol.*, **356**, 97–110.

39. Baker,B.J., Tyson,G.W., Webb,R.I., Flanagan,J., Hugenholtz,P., Allen,E.E. and Banfield,J.F. (2006) Lineages of acidophilic archaea revealed by community genomic analysis. *Science*, **314**, 1933–1935.

40. Palenchar,P.M., Buck,C.J., Cheng,H., Larson,T.J. and Mueller,E.G. (2000) Evidence that ThiI, an enzyme shared between thiamin and 4-thiouridine biosynthesis, may be a sulfurtransferase that proceeds through a persulfide intermediate. *J. Biol. Chem.*, **275**, 8283–8286.

41. Tanaka,Y., Yamagata,S., Kitago,Y., Yamada,Y., Chimnaronk,S., Yao,M. and Tanaka,I. (2009) Deduced RNA binding mechanism of ThiI based on structural and binding analyses of a minimal RNA ligand. *RNA*, **15**, 1498–1506.

42. Lauhon,C.T., Erwin,W.M. and Ton,G.N. (2004) Substrate specificity for 4-thiouridine modification in *Escherichia coli*. *J. Biol. Chem.*, **279**, 23022–23029.

43. Neumann,P., Lakomek,K., Naumann,P.T., Erwin,W.M., Lauhon,C.T. and Ficner,R. (2014) Crystal structure of a 4-thiouridine synthetase-RNA complex reveals specificity of tRNA U8 modification. *Nucleic Acids Res.*, **42**, 6673–6685.

44. Atomi,H., Fukui,T., Kanai,T., Morikawa,M. and Imanaka,T. (2004) Description of *Thermococcus kodakaraensis* sp. nov., a well studied hyperthermophilic archaeon previously reported as Pyrococcus sp. KOD1. *Archaea*, **1**, 263–267.

45. Fukui,T., Atomi,H., Kanai,T., Matsumi,R., Fujiwara,S. and Imanaka,T. (2005) Complete genome sequence of the hyperthermophilic archaeon *Thermococcus kodakaraensis* KOD1 and comparison with Pyrococcus genomes. *Genome Res.*, **15**, 352–363.

46. Doublié,S. (1997) Preparation of selenomethionyl proteins for phase determination. *Methods Enzymol.*, **276**, 523–530.

47. Otwinowski,Z. and Minor,W. (1997) Processing of X-ray Diffraction Data collected in oscillation mode. *Methods in Enzymol.*, **276**, 307–326.

48. Adams,P., Grosse-Kunstleve,R., Hung,L., Ioerger,T., McCoy,A., Moriarty,N., Read,R., Sacchettini,J., Sauter,N. and Terwilliger,T. (2002) PHENIX: building new software for automated crystallographic structure determination. *Acta Crystallogr D Biol. Crystallogr.*, **58**, 1948–1954.

49. Terwilliger,T.C. (2003) Automated side-chain model building and sequence assignment by template matching. *Acta Crystallogr D Biol. Crystallogr.*, **59**, 45–49.

50. Emsley,P. and Cowtan,K. (2004) Coot: model-building tools for molecular graphics. *Acta Crystallogr D Biol. Crystallogr.*, **60**, 2126–2132.

51. McCoy,A., Grosse-Kunstleve,R., Adams,P., Winn,M., Storoni,L. and Read,R. (2007) Phaser crystallographic software. *J. Appl. Crystallogr.*, **40**, 658–674.

52. Laskowski,R., MacArthur,M., Moss,D. and Thoronton,J. (1992) PROCHECK: a program to check the stereochemical quality of protein structures. *J. Appl. Cryst.*, **26**, 283–291.

53. Hori,H., Suzuki,T., Sugawara,K., Inoue,Y., Shibata,T., Kuramitsu,S., Yokoyama,S., Oshima,T. and Watanabe,K. (2002) Identification and characterization of tRNA (Gm18) methyltransferase from *Thermus thermophilus* HB8: domain structure and conserved amino acid sequence motifs. *Genes Cells.*, **7**, 259–272.

54. Keith,G. (1995) Mobilities of modified ribonucleotides on two-dimensional cellulose thin-layer chromatography. *Biochimie.*, **77**, 142–144.

55. Awai,T., Kimura,S., Tomikawa,C., Ochi,A., Ihsanawati,Bessho, Y., Yokoyama,S., Ohno,S., Nishikawa,K., Yokogawa,T. *et al.* (2009) *Aquifex aeolicus* tRNA (N^2,N^2-guanine)-dimethyltransferase (Trm1) catalyzes transfer of methyl groups not only to guanine 26 but also to guanine 27 in tRNA. *J. Biol. Chem.*, **284**, 20467–20478.

56. Baker,N., Sept,D., Joseph,S., Holst,M. and McCammon,J. (2001) Electrostatics of nanosystems: application to microtubules and the ribosome. *Proc. Natl. Acad. Sci. U.S.A.*, **98**, 10037–10041.

57. Wallace,A.C., Laskowski,R.A. and Thornton,J.M. (1995) LIGPLOT: a program to generate schematic diagrams of protein-ligand interactions. *Protein Eng.*, **8**, 127–134.

58. Chenna,R., Sugawara,H., Koike,T., Lopez,R., Gibson,T., Higgins,D. and Thompson,J. (2003) Multiple sequence alignment with the Clustal series of programs. *Nucleic Acids Res.*, **31**, 3497–3500.

59. Gouet,P., Robert,X. and Courcelle,E. (2003) ESPript/ENDscript: Extracting and rendering sequence and 3D information from atomic structures of proteins. *Nucleic Acids Res.*, **31**, 3320–3323.

60. Holm,L. and Rosenström,P. (2010) Dali server: conservation mapping in 3D. *Nucleic Acids Res.*, **38**, W545–W549.

61. Schluckebier,G., Kozak,M., Bleimling,N., Weinhold,E. and Saenger,W. (1997) Differential binding of S-adenosylmethionine S-adenosylhomocysteine and Sinefungin to the adenine-specific DNA methyltransferase M.TaqI. *J. Mol. Biol.*, **265**, 56–67.

62. Malone,T., Blumenthal,R.M. and Cheng,X. (1995) Structure-guided analysis reveals nine sequence motifs conserved among DNA amino-methyltransferases, and suggests a catalytic mechanism for these enzymes. *J. Mol. Biol.*, **253**, 618–632.

63. Demirci,H., Gregory,S.T., Dahlberg,A.E. and Jogl,G. (2008) Crystal structure of the Thermus thermophilus 16 S rRNA methyltransferase RsmC in complex with cofactor and substrate guanosine. *J. Biol. Chem.*, **283**, 26548–26556.

64. Laskowski,R.A. and Swindells,M.B. (2011) LigPlot+: multiple ligand-protein interaction diagrams for drug discovery. *J. Chem. Inf. Model.*, **51**, 2778–2786.